

LASERS

https://doi.org/10.1070/QEL16829

Efficient carrier transport in GRIN-SCH transistor lasers

M. Hosseini, H. Kaatuzian, I. Taghavi, H. Ghodsi

Abstract. **We report analytical and theoretical results of simulation of a graded-base, single quantum well (SQW) transistor laser (TL). Using an appropriate carrier transport model, device performances for different confinement structures are studies. Physical parameters including the diffusion constant and optical confinement factor are calculated, and the dependence of the optical response on both current level and structure design (e.g. base doping and cavity length) is investigated. Simulation results show that using graded index layers of $Al_{\xi}Ga_{1-\xi}As$ (ξ: 0.1→0) in the left-hand side of the QW and $Al_{\xi}Ga_{1-\xi}As$ (ξ: 0.05→0) in the right-hand side of the QW (instead of GaAs in the base region) increases the optical output power by a factor of 3, eliminates completely the resonance peak, and most interestingly increases optical bandwidth by ∼37% compared to the conventional (i.e. non-graded base) structure.**

Keywords: *transistor laser, graded index confinement structure, differential laser output, optical response, resonance peak.*

1. Introduction

A light-emitting transistor (LET) was introduced more than a decade ago [1] by extracting radiative recombination in the base layer of a heterojunction bipolar transistor (HBT). Incorporating one (or a few) quantum well(s) (QW) in the base region of the LET, one can achieve a high level of carrier recombination [2]. Continuous wave three-port (one electrical input, one electrical output, and one optical output) operation of such a device [called transistor laser (TL)] at room-temperature was first reported in [3].

The base region is critical to the transistor and all its versions including the TL, as it contains an active region from which stimulated recombination is extracted for laser operation [4]. Among versatile properties of the active region, the QW transit time (from the emitter to the QW) and active region transit time (from the emitter to the TL collector) are of key importance for the quantum well laser operation [5]. Other parameters, like QW dislocation, QW width and base width variation, have previously been investigated by the authors [6–9]. Carrier transit times across the separate confinement heterostructure (SCH) in the active region (base) in a single quantum well (SQW) TL is demonstrated in Fig. 1.

M. Hosseini, H. Kaatuzian, I. Taghavi, H. Ghodsi Photonics Research Laboratory, Electrical Engineering Department, Amirkabir University of Technology, Hafez Ave., Tehran, Iran; e-mail: hsnkato@aut.ac.ir

Received 28 September 2018; revision received 11 January 2019
Kvantovaya Elektronika **49** (4) 391–398 (2019)
Submitted in English

The carrier transport time through the left SCH region is comparatively longer in the HBTL than in the diode laser (DL) with the same SCH width because of a higher diffusion constant [10]. In order to maximise the modulation bandwidth of a quantum well laser, the carrier transit time across the SCH should be somehow minimised. One proposed method is based on utilising a graded index (GRIN) structure for the SCH which results in a built-in field and consequently a reduced transit time [5, 11]. Establishing the above-mentioned built-in quasi-electric field, the current flow includes a drift component in addition to diffusion component which in turn reduces the transit time.

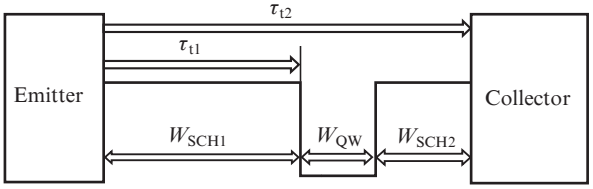

Figure 1. Schematic of the carrier transport through the SCH in the base region.

The effects of the graded base on the transit time have been already investigated both theoretically and experimentally in HBTs [12, 13] as well as in quantum well lasers [14, 15]. However, theoretical estimation of these effects on various optical and electrical characteristics of the transistor laser, with potential applications in tailoring this three-port device, has not been studied. Feng et al. [16] have already reported a 2.5 ps carrier recombination lifetime for a conventional transistor laser. We show here, however, that even a sub-picosecond carrier lifetime is achievable when a well-designed graded-base region is utilised.

In the present paper, we consider a GRIN-SCH structure by using $Al_{\xi}Ga_{1-\xi}As$ instead of GaAs in the SQW-TL. The energy gap (in eV) of the $Al_{\xi}Ga_{1-\xi}As$ material at $\xi < 0.45$ is determined as $E_g(Al_{\xi}Ga_{1-\xi}As) = 1.424 + 1.247\xi$, and the induced built-in potential can be achieved using $\varepsilon = \Delta E_g \times (qW_{SCH})^{-1}$, where W_{SCH} is the SCH width, ΔE_g is the bandgap energy difference at two sides of SCH regions and q is the electron charge. Using $Al_{\xi}Ga_{1-\xi}As$ (ξ: 0.1→0) in SCH1 and $Al_{\xi}Ga_{1-\xi}As$ (ξ: 0.05→0) in SCH2 yields $\varepsilon \approx 21$ and 22 kV cm^{-1}, respectively. These values of quasi-electric fields are in good agreement with the experimental values reported in the literature [12, 13]. To make it clear and show the effects of the graded index in the SCH regions separately, we investigate different confinement structures in the SQW TL. In

Section 2 we introduce band alignments of different structures and epitaxial layers of the GRIN-SCH SQW TL. An analytical model to describe GRIN effects in SCHs are considered in Section 3. In section 4 we discuss the base recombination lifetime, the differential laser output and the optical frequency response for different structures.

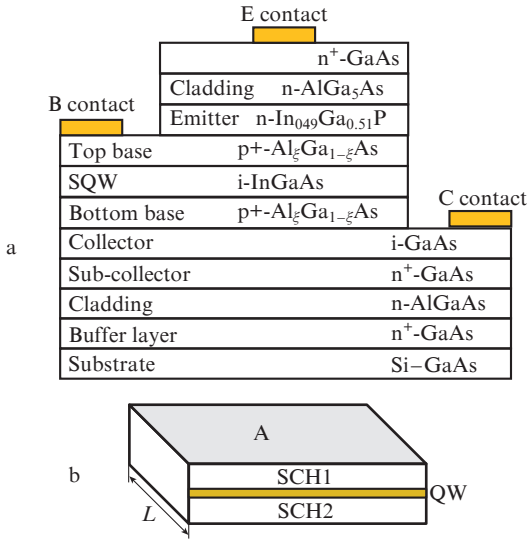

Figure 2. (a) Schematic diagram of the epitaxial structure of the crystal used for the GRIN-SCH HBTL and (b) geometry of the laser resonator.

2. Confinement structures

The epitaxial structure and fabrication process of the primary HBTL in question have been entirely described in Refs [3, 4]. The TL is based on the n–p–n HBT (n-InGaP/p-GaAs/n-GaAs) in which the base electric field is usually established by linearly grading the aluminium (or indium) content in the AlGaAs (or InGaAs) base [17]. The newly proposed graded-base HBTL structure, called the GRIN-SCH SQW TL, is shown in Fig. 2a. Figure 2b shows the geometry of the laser resonator. Compared to the original TL structure in [3], we did not alter the structure of the whole device except for SCH1 and SCH2. Our focus in this paper is the changes in the SCH rather than in the active region (i.e. QW).

In this paper, we investigate different confinement structures. The first structure is the conventional GaAs base TL (Fig. 3a), while in the second structure, we use a graded index $Al_{\xi}Ga_{1-\xi}As$ layer (ξ: 0.05→0) only in SCH2 (Fig. 3b). Similarly, we use a graded index $Al_{\xi}Ga_{1-\xi}As$ layer (ξ: 0.1→0) only in SCH1 (Fig. 3c) in the third structure. Finally, in the fourth structure graded index SCH1 and SCH2 are used simultaneously, i.e. $Al_{\xi}Ga_{1-\xi}As$ (ξ: 0.1→0) in SCH1 and $Al_{\xi}Ga_{1-\xi}As$ (ξ: 0.05→0) in SCH2 (Fig. 3d). Schematic band diagrams of these structures are shown in Fig. 3.

3. Model

As mentioned before and shown in Figs 2 and 3, the base region in the TL is composed of three series sections, namely

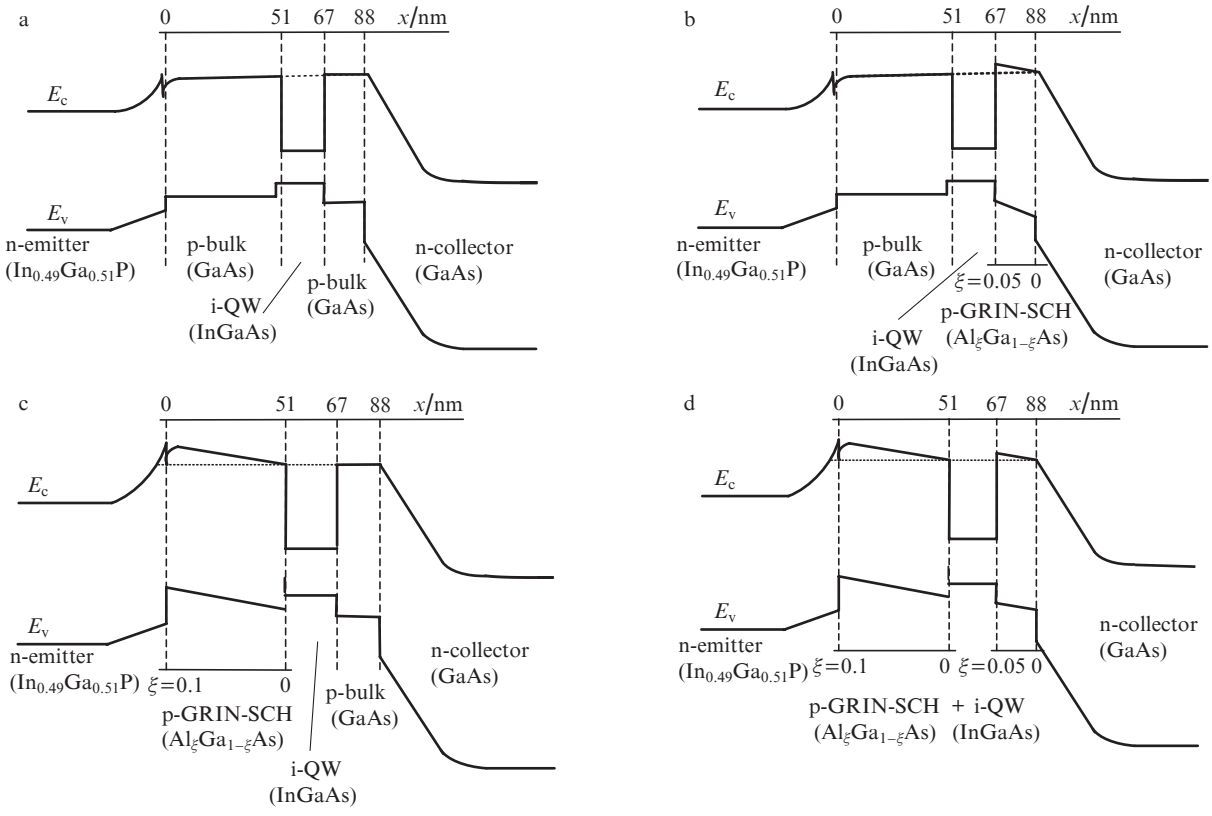

Figure 3. Schematic band diagrams of different confinement structures under forward bias: (a) structure 1, conventional GaAs base TL, (b) GRIN-SCH structure 2 with a graded index only in SCH2, (c) GRIN-SCH structure 3 with a graded index only in SCH1, (d) GRIN-SCH structure 4 with a graded index in SCH1 and SCH2 simultaneously.

SCH1, QW, and SCH2. The continuity equations in these regions for the original TL (with a non-graded base) have the form [16]

$$\frac{\partial n}{\partial t} = D\frac{\partial^2 n}{\partial x^2} - \frac{n}{\tau_{\text{bulk}}} \tag{1}$$

for SCH1 and SCH2 and

$$\frac{\partial n}{\partial t} = D\frac{\partial^2 n}{\partial x^2} - \frac{n}{\tau_{\text{QW}}} \tag{2}$$

for the QW, where $n(x,t)$ is the electron distribution in the base; D is the diffusion constant; and τ_{bulk} and τ_{QW} are recombination lifetimes in the bulk base and QW, respectively. In the charge control model, the current $I = qAD(\partial n/\partial \text{x})$ is assumed to be continuous across the SCH1/QW/SCH2 interfaces. In GRIN-SCH structures, due to the quasi-electric field, the base and collector current consist of both diffusion and the drift components:

$$I_{\text{b}} = -qAD\frac{\partial n_{\text{eQW}}}{\partial x} + qA\mu_{\text{n}} n_{\text{eQW}}(x)\varepsilon_{\text{b1}},\ 0 \leqslant x \leqslant W_{\text{eQW}}, \tag{3}$$

$$\begin{aligned} I_{\text{c}} &= -qAD\frac{\partial n_{\text{ce}}}{\partial x} + qA\mu_{\text{n}} n_{\text{ce}}(x)\varepsilon_{\text{b1}},\ 0 \leqslant x \leqslant W_{\text{eQW}}, \\ I_{\text{c}} &= -qAD\frac{\partial n_{\text{ce}}}{\partial x} + qA\mu_{\text{n}} n_{\text{ce}}(x)\varepsilon_{\text{b2}},\ W_{\text{eQW}} \leqslant x \leqslant W_{\text{ce}}, \end{aligned} \tag{4}$$

where W_{eQW} is the distance from the emitter junction up to the middle of the QW; W_{ce} is the collector junction distance from the emitter (base width); n_{eQW} is the base electron distribution that recombine in the QW and constitutes diffusion component of the base current; n_{ce} is the base electron distribution that transits from the base region (does not recombine in the QW) and constitutes diffusion component of the collector current; ε_{b1} and ε_{b2} are the quasi-electric fields in SCH1 and SCH2 respectively; μ_{n} is the minority electron mobility in the base region; and A is the emitter area. If we neglect the recombination outside of the QW ($\tau_{\text{bulk}} \gg \tau_{\text{QW}}$) [16], then I_{b} and I_{c} are constant across the base region.

By assuming a zero charge density at the base–collector junction and continuity of the carrier density across the base, we can solve equations (1)–(4) analytically:

$$n_{\text{eQW}}(x) = \frac{I_{\text{b}} W_{\text{eQW}}}{qAD}\frac{1}{k_1}\left\{1 - \exp\left[-k_1\left(1 - \frac{x}{W_{\text{eQW}}}\right)\right]\right\},\quad 0 \leqslant x \leqslant W_{\text{eQW}}, \tag{5}$$

$$\begin{aligned} n_{\text{ce}}(x) &= \frac{I_{\text{c}} W_{\text{eQW}}}{qAD}\frac{1}{k_1}\left\{1 - \exp\left[-k_1\left(1 - \frac{x}{W_{\text{eQW}}}\right)\right]\right\} \\ &\quad + n_0 \exp\left[-k_1\left(1 - \frac{x}{W_{\text{eQW}}}\right)\right],\ 0 \leqslant x \leqslant W_{\text{eQW}}, \\ n_{\text{ce}}(x) &= \frac{I_{\text{c}} W_{\text{QWc}}}{qAD}\frac{1}{k_2}\left\{1 - \exp\left[-k_2\left(1 + \frac{W_{\text{eQW}} - x}{W_{\text{QWc}}}\right)\right]\right\}, \\ &\quad W_{\text{eQW}} \leqslant x \leqslant W_{\text{ce}}, \end{aligned} \tag{6}$$

where $k_1 = [q\varepsilon_{\text{b1}}/(kT)]W_{\text{SCH1}} = \Delta E_{\text{g1}}/(kT)$ and $k_2 = [q\varepsilon_{\text{b2}} \times (kT)^{-1}]W_{\text{SCH2}} = \Delta E_{\text{g2}}(kT)^{-1}$ are the SCH1 and SCH2 electric factor, respectively; $n_0 = [I_{\text{c}} W_{\text{QWc}}/(qADk_2)][1 - \exp(-k_2)]$ is a constant; ΔE_{g1} and ΔE_{g2} are the bandgap energy differences at the two sides of SCHs; and W_{QWc} is the distance from the QW to the collector..

The transit time from the emitter to the quantum well (τ_{t1}) and from the emitter to the collector (τ_{t2}) can be expressed as:

$$\tau_{\text{t1}} = Q_1 I_{\text{b}}^{-1} = qA\int_0^{W_{\text{eQW}}} n_{\text{eQW}}(x)\,\text{d}x I_{\text{b}}^{-1}, \tag{7}$$

$$\tau_{\text{t2}} = Q_2 I_{\text{c}}^{-1} = qA\int_0^{W_{\text{ce}}} n_{\text{ce}}(x)\,\text{d}x I_{\text{c}}^{-1}, \tag{8}$$

where Q_1 and Q_2 are the base charges produced by n_{eQW} and n_{ce}, respectively. The overall effective base recombination lifetime can be expressed as:

$$\tau_{\text{b}} = \frac{Q_1 + Q_2}{I_{\text{b}}} = \frac{Q_1 + Q_2}{\dfrac{Q_1}{\tau_{\text{t1}}} + \dfrac{Q_1 + Q_2}{\tau_{\text{bulk}}}} \approx \left(1 + \frac{Q_2}{Q_1}\right)\tau_{\text{t1}}. \tag{9}$$

4. Simulation parameters

To simulatethe device, we need to calculate some of its optical and structural parameters in advance. All of these primary calculations along with DC and AC analysis of the device are performed within a set of self-consistent codes using MATLAB.

4.1. Diffusion constant

Minority electron mobility in $\text{Al}_\xi\text{Ga}_{1-\xi}\text{As}$ ($0 \leqslant \xi \leqslant 0.3$) for donor densities between 10^{16} and 10^{19} cm^{-3} were calculated by Herbert [18], and the results are in good agreement with the experiment. Extracted values of electron mobilities for different donor densities are shown in Fig. 4a. For the first order analysis (with good agreement with the experimental results), the effective minority electron mobility, $\mu_{\text{n}}^{\text{eff}}$, in the base region, for different confinement structures is defined [19]

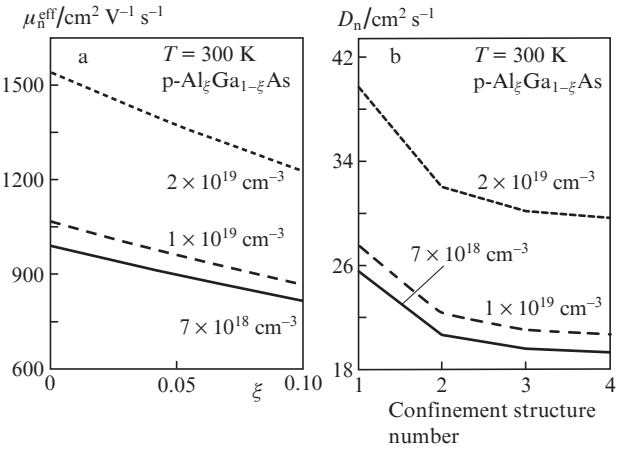

Figure 4. (a) Extracted minority electron mobility in $\text{Al}_\xi\text{Ga}_{1-\xi}\text{As}$ ($0 \leqslant \xi \leqslant 0.1$) for different acceptor densities [18] and (b) calculated values of the diffusion constant for different confinement structures.

$$\mu_{\mathrm{n}}^{\mathrm{eff}} = \frac{\mu_{\mathrm{nSCH1}}^{\mathrm{avg}} W_{\mathrm{SCH1}} + \mu_{\mathrm{nSCH2}}^{\mathrm{avg}} W_{\mathrm{SCH2}}}{W_{\mathrm{SCH1}} + W_{\mathrm{SCH21}}}. \quad (10)$$

The diffusion constant can be obtained using an approximation of the Joyce–Dixon equation by Einstein formula [17]:

$$D_{\mathrm{n}} = \mu_{\mathrm{n}}^{\mathrm{eff}} \frac{kT}{q}. \quad (11)$$

The calculated values of the diffusion constant for different confinement structures versus the base doping are shown in Fig. 4b.

4.2. Optical confinement factor

The optical confinement factor (OCF) for the transistor laser was calculated analytically in [10]. The refractive index profile of the GRIN-SCH SQW TL is depicted in Fig. 5a. The effective refractive index of the waveguide can be defined as

$$n_{\mathrm{eff}} = \frac{W_{\mathrm{SCH1}} n_{\mathrm{SCH1}}^{\mathrm{avg}} + W_{\mathrm{QW}} n_{\mathrm{QW}} + W_{\mathrm{SCH2}} n_{\mathrm{SCH2}}^{\mathrm{avg}}}{W_{\mathrm{b}}}, \quad (12)$$

where $n_{\mathrm{SCH1}}^{\mathrm{avg}}$, $n_{\mathrm{SCH2}}^{\mathrm{avg}}$ and n_{QW} are the refractive indices; and $W_{\mathrm{b}} = W_{\mathrm{SCH1}} + W_{\mathrm{QW}} + W_{\mathrm{SCH2}}$. The normalised thickness of the optical waveguide can be described as

$$\Delta = \frac{2\pi}{\lambda_0} W_{\mathrm{b}} \sqrt{n_{\mathrm{eff}}^2 - n_{\mathrm{clad}}^2}. \quad (13)$$

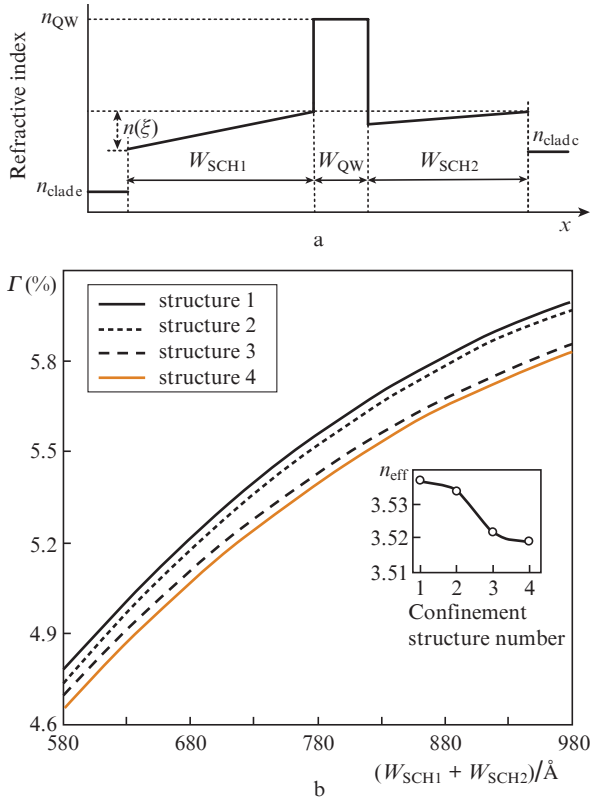

Figure 5. (a) Refractive index profile of the GRIN-SCH SQW TL and (b) optical confinement factor for structures 1–4. The inset shows effective refractive indices of the waveguide for different structures (the QW width is 16nm and is constant and the SCH width is variable).

With allowance for different cladding materials in the HBTL, we used for these layers an average refractive index

$$n_{\mathrm{clad}} = \frac{n_{\mathrm{clade}} + n_{\mathrm{cladc}}}{2}. \quad (14)$$

The optical confinement factor Γ can thus be estimated as

$$\Gamma \approx \frac{1}{1 + 2/\Delta^2} \frac{W_{\mathrm{QW}}}{W_{\mathrm{b}}}.$$

Figure 5b shows the calculated OCF for all three structures, and the inset shows the values of the effective refractive index of the waveguide for different structures. The total optical loss for this structure is composed of two terms: the cavity-dependent mirror loss, α_{m}, and doping-dependent intrinsic optical loss, α_{i}:

$$\alpha_{\mathrm{m}} = \frac{1}{2L} \ln \frac{1}{R_1 R_2}, \quad (16)$$

$$\alpha_{\mathrm{i}} = \Gamma k_{\mathrm{p}} N_{\mathrm{b}}, \quad (17)$$

where L is the laser cavity length; $R_{1,2}$ are the reflectivities of the cavity mirrors; k_{p} is intervalence band absorption coefficient; and N_{b} is the base doping concentration. The photon lifetime, τ_{ph}, can therefore be calculated by the formula

$$\tau_{\mathrm{ph}} = \left[\frac{c}{n_{\mathrm{wg}}}(\alpha_{\mathrm{m}} + \alpha_{\mathrm{i}})\right]^{-1}, \quad (18)$$

where n_{wg} is the refractive index of the waveguide.

5. Results and discussion

The numerical values used in the model are summarised below.

Base width, W_{ce}/Å	880 [16]
QW distance from emitter junction, W_{eQW}/Å	590 [16]
QW distance from collector junction, W_{QWc}/Å	290 [16]
QW width, W_{QW}/Å	160 [16]
Bulk recombination lifetime, τ_{bulk}/ps	134 [4]
Base doping concentration, N_{b}/cm^{-3}	1×10^{19}
Temperature, T/K	300
Boltzmann constant, k/eV K^{-1}	8.617×10^{-5}
Emitter area, A/μm^2	120×120
Laser cavity length, L/μm	450
External quantum efficiency, η_{ext}	0.1 [20]
Fitting parameter, η	0.1 [20]

5.1. DC performance

Figure 6 shows the minority carrier distributions in the TL base, calculated by Eqns (5) and (6) for increasing base currents in different structures. The results in Fig. 6a correspond to a conventional GaAs base transistor laser. In this structure, there is no quasi-electric field, and so the minority carrier distribution is constantly tilted in both SCH regions. Figure 6b illustrates the carrier distribution

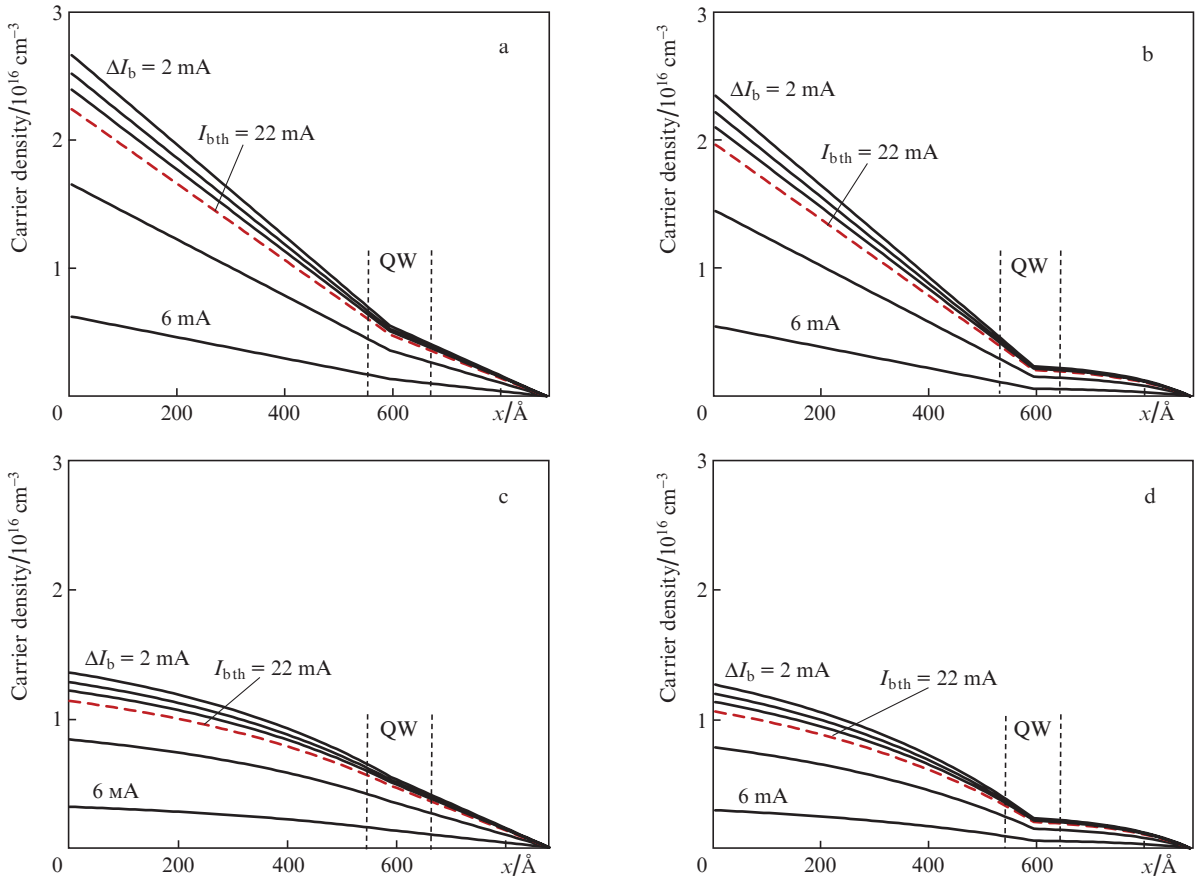

Figure 6. Calculated minority carrier (electron) distributions for different GRIN-SCH structures of Fig. 3.

in structure 2; as it turns out, there is a variaable tilt in SCH2 only due to the quasi-electric field in this region. In the same way, in Fig. 6c, related to structure 3 (Fig. 3c), a variable tilt exists only in SCH1. Finally, Fig. 6d demonstrates the carrier distribution where tilting is apparent all across the base (except the active region) due to the quasi-electric field in both SCHs.

Figure 7 shows the corresponding calculated effective base recombination lifetimes, τ_b, for each structure. Using the GRIN-SCH structure, the overall effective base recombination lifetime τ_b can be significantly reduced. Apparently, the recombination lifetime is related to transit times across SCHs (τ_{t1} and τ_{t2}) and charge populations Q_1 and Q_2.

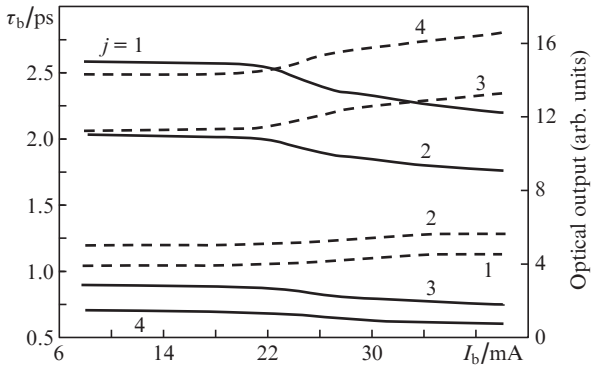

Figure 7. Calculated overall effective base recombination lifetimes τ_b (solid curves), and optical output (dashed curves) for the charge distributions shown in Fig. 6; j is the number of the confinement structure.

Simulation results for transit times in different structures and current gains as well as the dependences of the transit time on the aluminium mole fraction in the graded index $Al_\xi Ga_{1-\xi}As$ layers are shown in Figs 8a and 8b. Evidently, the change in the transit time from structure 1 to structure 2 is not prominent due to the location of the QW. However, one can drastically reduce this transit time by grading SCH1 as it is wider than SCH2. Similarly, the improvement from structure 3 to 4 is not so high to pay off the difficulties in fabrication.

For the QW transistor laser with stimulated base recombination, the small signal current gain, $\beta = \Delta I_c/\Delta I_b$ can be expressed as $\beta = \tau_b/\tau_t$ [4], where τ_b is the overall effective base recombination lifetime that can be achieved using Eqn (9) and τ_t denotes the base transit time. The current gain for all structures is depicted in Fig. 8b. As it can be seen there is no significant difference in the current gain values between original and proposed GRIN-SCH structures because of a slight variation of the base recombination lifetime. The effect of SCH1 can be observed by comparing Fig. 8c with Fig. 8d. As a conclusion, both SCH regions' width and the QW (or QWs) location are among critical factors in designing a TL since in the HBTL only carriers of one types are transported. This is in contrast to the case of a conventional diode laser in which both carriers (apparently with different velocities) are transported through SCH regions, resulting in a more nonuniform carrier distribution. Our simulation results show this advantage of the TL compared to the DL.

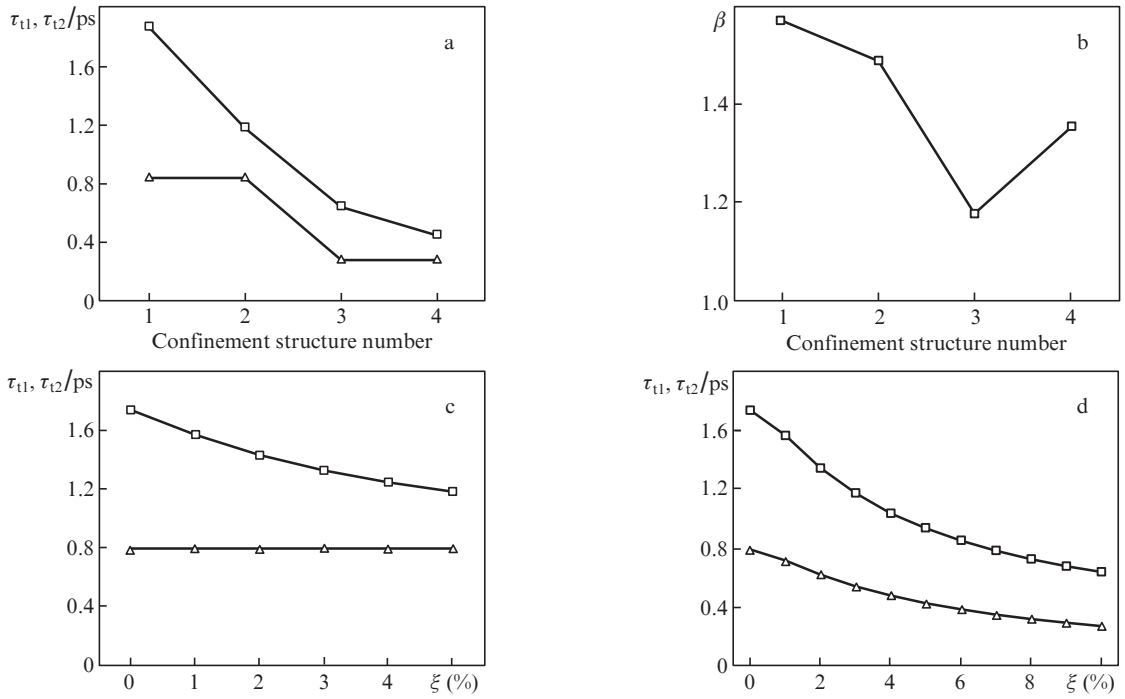

Figure 8. (a) Transit times, τ_{t1} (triangles) and τ_{t2} (squares), in different structures; (b) small signal current gain β in different structures; and (c, d) dependences of the transit times on the Al mole fraction in (c) SCH2 (structure 2) and (d) SCH1 (structure 3).

By extracting Q_1 and Q_2 from Fig. 6 and using Eqn (9) at a threshold current I_{th}, we can obtain the spontaneous recombination lifetime τ_{bspon} for structures 2–4. The dependence of the spontaneous recombination lifetime on the aluminium mole fraction in SCHs is depicted in Fig. 9 and can be also treated as an extra proof that SCH1 (which is located prior to the active region) has a more important effect on the overall performance of the device. It is worth noting that τ_{bspon} can directly alter the optical modulation bandwidth of the TL.

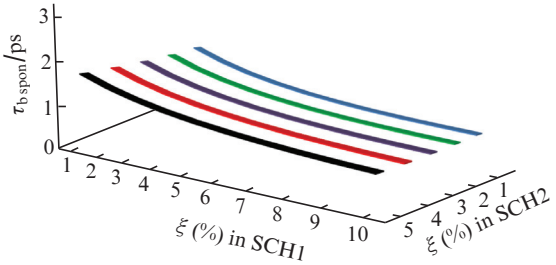

Figure 9. Dependence of the spontaneous recombination lifetime, τ_{bspon}, on the aluminium mole fractions ξ in SCH1 and SCH 2.

An expression for the effective differential laser output with respect to a change in the carrier density N has been obtained in [21]

$$\frac{1}{v_g P}\frac{dR_{st}}{dN} = \frac{q\alpha_m}{\eta_{ext}}\left(\frac{1}{\tau_b} - \frac{1}{\tau_{bspon}}\right)\frac{W_b}{I_b - I_{bth}}, \quad (19)$$

where η_{ext} is the external quantum efficiency; R_{st} is the stimulated recombination rate; v_g is the photon group velocity; and P is the cavity photon population density. Figure 10 shows the effective differential laser output for the proposed structures. The highest optical output can be observed in structure 4 due to its minimum base recombination lifetime. For $I_b < I_{bth}$, the stimulated recombination is negligible, and consequently, the recombination rate can be negelected.

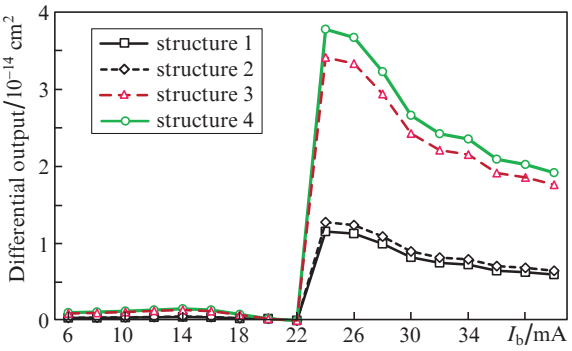

Figure 10. Effective differential laser output for different structures.

5.2. AC performance

Laser rate equations for the TL can be obtained from a modification of the coupled carrier-photon equations

$$\frac{dN}{dt} = \frac{I_b}{q} - \frac{N}{\tau_{bspon}} - v_g g \Gamma N_{ph}, \quad (20)$$

$$\frac{dN_{ph}}{dt} = v_g g \Gamma N_{ph} - \frac{N_{ph}}{\tau_{ph}}, \quad (21)$$

where $N \approx (Q_1 + Q_2)/q$ is the total base minority carrier population; g is the gain per unit length of the active medium (QW); and N_{ph} is the total number of photons. For the small-signal linear optical response we obtain an analytical equation [22]

$$H(\omega) = \frac{A_0}{1 - \omega^2/\omega_n^2 + i2(\omega/\omega_n)\zeta},$$

where

$$\zeta = \frac{1}{2\omega_n \tau_{bspon}} + \frac{\tau_{ph}\omega_n}{2}; \quad \omega_n^2 = \frac{\eta}{\tau_{ph}\tau_{bspon}}\left(\frac{I_b}{I_{bth}} - 1\right);$$

A_0 is a normalisation factor; $\omega_r = \omega_n/(1 - 2\zeta^2)^{1/2}$ is the resonance frequency; and η is a fitting parameter that has previously been calculated [20]. The magnitude of the resonance peak is $|H(\omega_r)|^2 = A_0^2/[4(1 - \zeta^2)\zeta^2]$.

Figure 11 shows the intrinsic optical frequency response of different confinement structures. The key factor of the optical frequency response in the TL is spontaneous recombination lifetime τ_{spon}, which is depicted as an inset in Fig. 11. With decreasing spontaneous recombination lifetime, the resonance peak decreases drastically and the optical bandwidth increases. As can be seen, no resonance peak is observed structure 3 and 4, which could be another potential advantage of this device. The resonance peak is mainly a limiting factor for optical transmitters based on direct modulation of diode lasers. It is expected that using a modified GRIN-SCH TL (preferably in structure 3 or 4) this issue could be resolved.

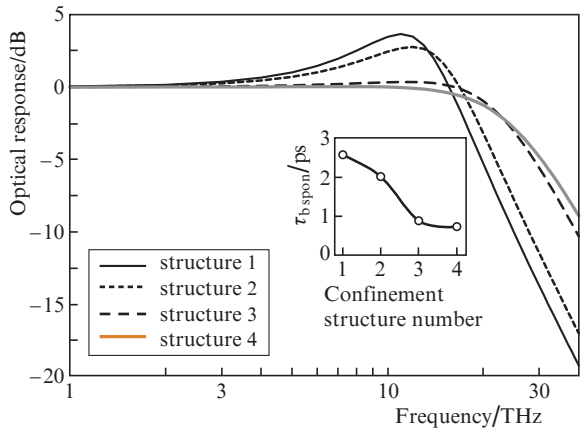

Figure 11. Optical response of GRIN-SCH structures and conventional GaAs base TL ($I_b/I_{bth} = 5$, $N_b = 1 \times 10^{19}$ cm^{-3}). The inset shows the values of the spontaneous recombination lifetime τ_{bspon} for all structures.

Figure 12 shows the optical bandwidth and the resonance peak of different structures versus different base doping. A higher bandwidth observed for structures 3 and 4 is a direct consequence of the resonance-free optical frequency response. Superior optical modulation performances (both in terms of a higher intrinsic bandwidth and a lower resonance peak) are evident in structures 3 and 4. When fully combined with other techniques for increasing the bandwidth including a multiple quantum well active region [10], it is anticipated that the final bandwidth could go beyond 100 GHz.

Varying the base current, we compared the optical performances of original TL and different GRIN-SCH structures in

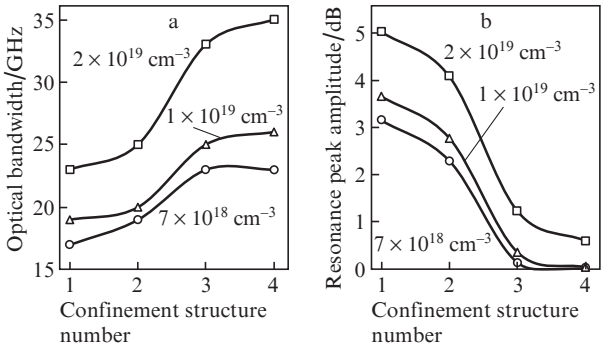

Figure 12. (a) Optical bandwidth and (b) resonance peak amplitude for different structures at different base dopings. In structure 3, the resonance peak is zero.

Fig. 13. Apparently, the original structure has a wider bandwidth compared to the proposed GRIN-SCH structures at a low current due to a higher rate of carriers captured by this structure. The bandwidth increases up to ~19 GHz for the original TL where saturation in the material gain limits it. In the GRIN-SCH case, bandwidth enhancement starts at relatively higher injection levels for which the QW is provided with high enough carriers and goes beyond 26 GHz.

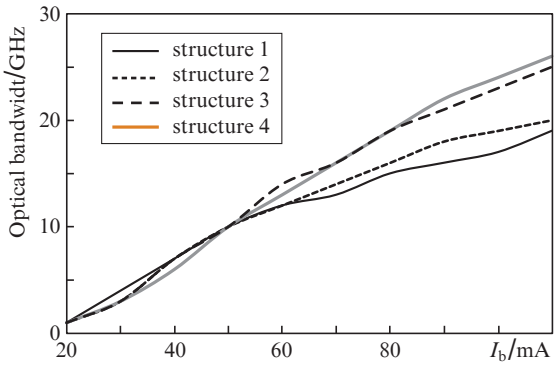

Figure 13. Dependence of the optical bandwidth on the base current for different confinement structures.

By employing a faster τ_{bspon}, the resonance-free condition can be attained even at low biases, because low N_{ph} and small τ_{bspon} lead to a large ζ. Moreover, the situation is reversed in that, with fast τ_{bspon}, the resonance appears only at large I_b/I_{bth} due to an increase in ω_n, which reduces ζ. The key parameter related to the optical bandwidth and cavity length is the photon lifetime τ_{ph}, which has previously been calculated taking into account the cavity-dependent mirror loss compared to doping-dependent intrinsic optical loss [7]. Structures 3 and 4 with a cavity length between 550 to 850 μm have the same optical bandwidth because of same values in photon lifetimes as it can be seen in Fig. 14. Combined with the effect of a graded base, one can conclude that sensitivity to the cavity length variations is more apparent in the GRIN-SCH TL compared to its conventional, non-graded version. This could be a disadvantage for our proposed grade base version of the TL that should be taken into consideration when fabrication limitations become more important. On the other hand, structures 3 and 4 show a 50% improvement in

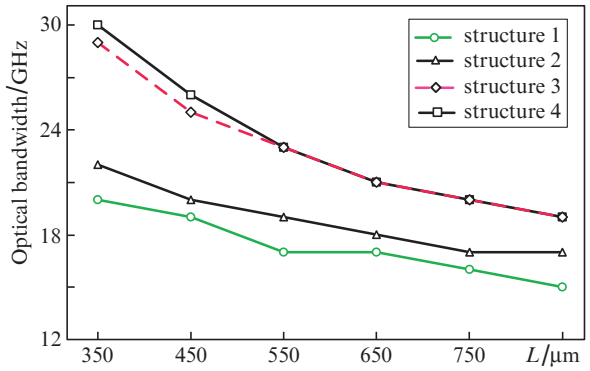

Figure 14. Dependence of the optical bandwidth on the cavity length for different confinement structures.

optical bandwidth for a relatively small cavity length of 350 μm.

6. Conclusions

We have studied for the first time a GRIN-SCH structure in a SQW transistor laser with different confinement structures. The key physical parameters of the proposed structures, including diffusion constant, optical confinement factor, transit time through SCHs, effective base recombination lifetime and charge density profile in the base region, have been calculated. Then, the TL characteristics including differential laser output and optical frequency response have been analysed for the proposed GRIN-SCH structures. Using the $Al_{\xi}Ga_{1-\xi}As$ (ξ: $0.1 \rightarrow 0$) in the left-hand side of the QW and $Al_{\xi}Ga_{1-\xi}As$ (ξ: $0.05 \rightarrow 0$) in the right-hand side of the QW, the differential laser output has been demonstrated to increase by a factor of 3. It has been shown that the resonance peak is eliminated completely and the optical bandwidth increases to 26 GHz compared to 19 GHz in conventional GaAs base TLs. We believe this higher optical bandwidth is a direct result of sub-picosecond base recombination lifetime thanks to accelerated carrier transport through the base region.

References

1. Feng M., Holonyak N. Jr, Hafez W. *Appl. Phys. Lett*., **84** (1), 151 (2004).
2. Walter G., Holonyak N. Jr, Feng M., Chan M. *Appl. Phys. Lett*., **85** (20), 4768 (2004).
3. Feng M., Holonyak N. Jr, Walter G., Chan R. *Appl. Phys. Lett*., **87**, 131103 (2005).
4. Chan R., Feng M., Holonyak N. Jr, James A., Walter G. *Appl. Phys. Lett*., **88**, 143508 (2006).
5. Nagarajan R., Fukushima T., Corzine S.W., Bower J.E. *Appl. Phys. Lett*., **59** (15), 1835 (1991).
6. Taghavi I., Kaatuzian H. *Opt. Quantum Electron*., **41**, 481 (2010), DOI: 10.1007/s11082-010-9384-0.
7. Farjadian M.R., Kaatuzian H., Taghavi I. *Opt. Quantum Electron*., **46**, 871 (2013).
8. Mojaver H.R., Kaatuzian H. *Opt. Quantum Electron*., **44**, 45 (2012), DOI: 10.1007/s11082-011-9531-2.
9. Hosseini M., Kaatuzian H., Taghavi I. *Proc. 24th Iranian Conf. Electrical Engineering (ICEE)* (Shiraz, 2016) pp 617–620, DOI: 10.1109/IranianCEE.2016.7585596.
10. Taghavi I., Kaatuzian H., Leburton J.P. *IEEE J. Quantum Electron*., **49** (4), 426 (2013).
11. Hosseini M., Kaatuzian H., Taghavi I. *Chin. Opt. Lett*., **15**, 062501 (2017).
12. Liu W., Costa D., Harris J. *IEEE Trans. Electron. Devices*, **39** (11), 2422 (1992).
13. Joe J.H., Missous M. *IEEE Trans. Electron. Devices*, **52** (8), 1693 (2005).
14. Morin S., Deveaud B., Clerot F., Fujiwara K., Mitsunaga K. *IEEE J. Quantum Electron*., **27** (6), 1669 (1991).
15. Polland H.-J., Leo K., Rother K., Ploog K., Feldmann J., Peter G., Göbel E.O., Fujiwara K., Nakayama T., Ohta Y. *Phys. Rev. B*, **38**, 7635 (1988).
16. Feng M., Holonyak N. Jr, Then H.W., Walter G. *Appl. Phys. Lett*., **91**, 053501 (2007).
17. Liu W. *Fundamentals of III–V Devices* (New York: Wiley, 1999).
18. Bennett H.S. *Appl. Phys*., **80**, 3844 (1996), DOI: 10.1063/1.363339.
19. Kaatuzian H. *Photonics* (Tehran: Amirkabir University (AKU) Press, 2017) Vol. 2.
20. Then H.W., Feng M., Holonyak N. Jr. *Appl. Phys. Lett*., **91**, 183505 (2007).
21. Then H.W., Walter G., Feng M., Holonyak N. Jr. *Appl. Phys. Lett*., **91**, 243508 (2007).
22. Feng M., Then H.W., Holonyak N. Jr, Walter G., James A. *Appl. Phys. Lett*., **95**, 033509 (2009).